JGR Oceans

RESEARCH ARTICLE
10.1029/2018JC014775

Unabated Bottom Water Warming and Freshening in the South Pacific Ocean

Sarah G. Purkey[1], Gregory C. Johnson[2], Lynne D. Talley[1], Bernadette M. Sloyan[3,4], Susan E. Wijffels[3,4,5], William Smethie[6], Sabine Mecking[7], and Katsuro Katsumata[8]

[1]Scripps Institution of Oceanography, University of California, San Diego, CA, USA, [2]NOAA/Pacific Marine Environmental Laboratory, Seattle, WA, USA, [3]Oceans and Atmosphere, CSIRO, Hobart, Tasmania, Australia, [4]Centre for Southern Hemisphere Oceans Research, Hobart, Tasmania, Australia, [5]Department of Physical Oceanography, Woods Hole Oceanographic Institution, Woods Hole, MA, USA, [6]Lamont-Doherty Earth Observatory, Columbia University, Palisades, NY, USA, [7]Applied Physics Laboratory, University of Washington, Seattle, WA, USA, [8]Research Institute for Global Change, JAMSTEC, Yokosuka, Japan

Key Points:
- Bottom waters in the South Pacific Ocean have warmed steadily since the 1990s, based on data from multiple repeat oceanographic transects
- Maximum warming of 0.04 degrees C/decade is found within the deep Ross Sea, with the signal weakening to the north
- Antarctic Bottom Water freshening, limited to around Antarctica in previous decades, has reached the Southwest Pacific Basin in the 2010s

Correspondence to:
S. G. Purkey,
spurkey@ucsd.edu

Citation:
Purkey, S. G., Johnson, G. C., Talley, L. D., Sloyan, B. M., Wijffels, S. E., Smethie, W., et al. (2019). Unabated bottom water warming and freshening in the South Pacific Ocean. *Journal of Geophysical Research: Oceans*, *124*, 1778–1794. https://doi.org/10.1029/2018JC014775

Received 15 NOV 2018
Accepted 18 FEB 2019
Accepted article online 20 FEB 2019
Published online 18 MAR 2019

Abstract Abyssal ocean warming contributed substantially to anthropogenic ocean heat uptake and global sea level rise between 1990 and 2010. In the 2010s, several hydrographic sections crossing the South Pacific Ocean were occupied for a third or fourth time since the 1990s, allowing for an assessment of the decadal variability in the local abyssal ocean properties among the 1990s, 2000s, and 2010s. These observations from three decades reveal steady to accelerated bottom water warming since the 1990s. Strong abyssal ($z > 4{,}000$ m) warming of 3.5 ($\pm$1.4) m°C/year (m°C = 10^{-3} °C) is observed in the Ross Sea, directly downstream from bottom water formation sites, with warming rates of 2.5 ($\pm$0.4) m°C/year to the east in the Amundsen-Bellingshausen Basin and 1.3 ($\pm$0.2) m°C/year to the north in the Southwest Pacific Basin, all associated with a bottom-intensified descent of the deepest isotherms. Warming is consistently found across all sections and their occupations within each basin, demonstrating that the abyssal warming is monotonic, basin-wide, and multidecadal. In addition, bottom water freshening was strongest in the Ross Sea, with smaller amplitude in the Amundsen-Bellingshausen Basin in the 2000s, but is discernible in portions of the Southwest Pacific Basin by the 2010s. These results indicate that bottom water freshening, stemming from strong freshening of Ross Shelf Waters, is being advected along deep isopycnals and mixed into deep basins, albeit on longer timescales than the dynamically driven, wave-propagated warming signal. We quantify the contribution of the warming to local sea level and heat budgets.

Plain Language Summary Over 90% of the excess energy gained by Earth's climate system has been absorbed by the oceans, with about 10% found deeper than 2,000 m. The rates and patterns of deep and abyssal (deeper than 4,000 m) ocean warming, while vital for understanding how this heat sink might behave in the future, are poorly known owing to limited data. Here we use highly accurate data collected by ships along oceanic transects with decadal revisits to quantify how much heat and freshwater has entered the South Pacific Ocean between the 1990s and 2010s. We find widespread warming throughout the deep basins there and evidence that the warming rate has accelerated in the 2010s relative to the 1990s. The warming is strongest near Antarctica where the abyssal ocean is ventilated by surface waters that sink to the sea floor and hence become bottom water, but abyssal warming is observed everywhere. In addition, we observe an infusion of freshwater propagating along the pathway of the bottom water as it moves northward from Antarctica. We quantify the deep ocean warming contributions to heat uptake as well as sea level rise through thermal expansion.

1. Introduction

The deep ($2{,}000 < z < 4{,}000$ m) and abyssal ($z > 4{,}000$ m) oceans warmed significantly between the 1990s and 2000s, storing some of the excess heat entering Earth's climate system and contributing to global sea level rise (SLR) through thermal expansion (Desbruyères et al., 2016; Kouketsu et al., 2011; Purkey & Johnson, 2010). The abyssal warming is concentrated in regions of the global ocean ventilated largely by Antarctic Bottom Water (AABW), a water mass primarily formed by entrainment and mixing processes as dense waters descend from the continental shelves to the deep and abyssal ocean (Johnson, 2008; Orsi et al., 1999). The magnitude of the rate of warming is strongest in the Southern Ocean near AABW formation sites and weakens, but is still significant, to the north. A global inventory of the deep and abyssal warming

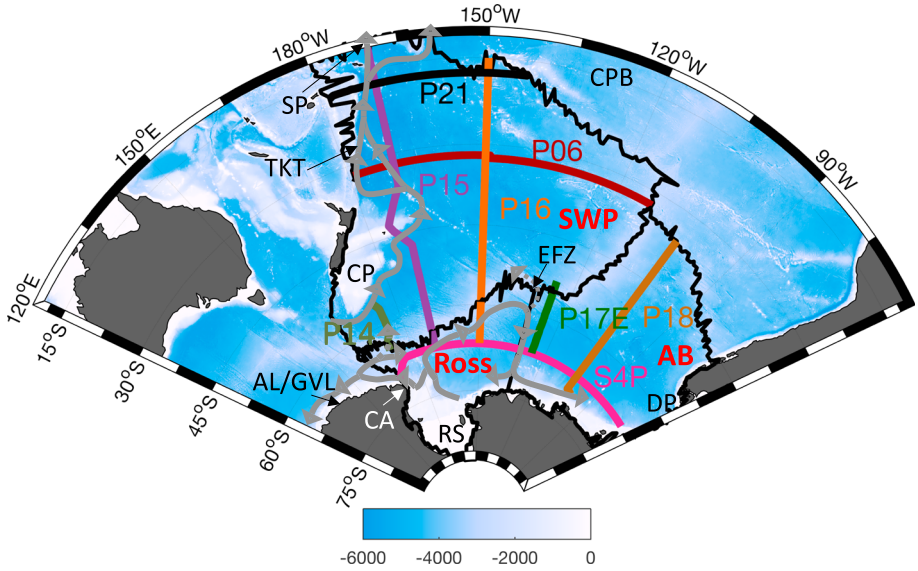

Figure 1. Track lines of the eight repeated sections with their designators (colors) within the Southwest Pacific Basin (SWP), the Ross Sea (Ross), and the Amundsen-Bellingshausen Basin (AB) labeled in red and outlined in black over the bottom bathymetry (Smith & Sandwell, 1997; color bar). Approximate locations of the Eltanin fracture zone (EFZ), Adélie Land/George V Land coast (AL/GVL), Ross Shelf (RS), Cape Adare (CA), Campbell Plateau (CP), Tonga-Kermadec Trench (TKT), Samoan Passage (SP), Central Pacific Basin (CPB), and Drakes Passage (DP) are labeled. Primary (solid gray) and secondary (dashed gray) pathways of Antarctic Bottom Water are indicated following Talley et al. (2011) and Orsi et al. (1999).

equates to a 0.07 W/m^2 average flux applied over Earth's surface area, taking up a substantial fraction of the total ~0.7 W/m^2 total global energy imbalance (Durack et al., 2018; Johnson et al., 2016; Palmer et al., 2017; Purkey & Johnson, 2010; Rhein et al., 2013).

The mechanisms driving the abyssal warming are expressed in changes to the volume and properties of AABW over the past decades. A useful framework is to distinguish where changes are owing to (i) an advective change, associated with a water mass change, for example, a change in the temperature and salinity of one or more of AABW's end members, or (ii) isopycnal displacement or "heave," reflecting a change in the volume of isopycnal layers (Bindoff & McDougall, 1994). In the abyss, this might be related to an imbalance between the rate of bottom water supply and the combined effects of mixing and geothermal heating (Purkey & Johnson, 2012). In the deep south Pacific ocean, warming is associated with a deepening or descent of the isopycnals. While water mass changes are constrained by advective time scales, which can be centennial or even millennial in the abyssal ocean far from AABW formation regions (Khatiwala et al., 2012), isopycnal displacement can be communicated throughout the global ocean by planetary waves over decades (Kawase, 1987; Kouketsu et al., 2009, 2011; Masuda et al., 2010). For example, an analysis of a data-assimilating model showed that observed warming at 4,000 m in the North Pacific can be traced back to a decline in bottom water production of AABW off the Adélie coast of Antarctica 50 years prior, communicated through coastal Kelvin and Rossby waves (Masuda et al., 2010). Furthermore, as the ventilation rate of AABW into the Southern Ocean decreases, it drives a downward isopycnal displacement near the sills constraining northward flow of AABW, thus reducing the supply of the coldest water to the basins to the north and driving a loss of the densest isopycnals along the abyssal outflow of AABW (Purkey & Johnson, 2012).

The two primary regions of AABW formation in the Indo-Pacific sector of the Southern Ocean are the Ross Shelf and the Adélie Land/George V Land coast (Orsi et al., 1999; Figure 1), both of which have experienced dramatic changes in the past decades. Ross Shelf waters have freshened at a rate of 0.003 year^{-1} since the 1950s, possibly owing to a flux of glacial melt water from west Antarctica over the time period (Jacobs, 2002; Jacobs & Giulivi, 2010). The shelf water mixes with Circumpolar Deep Water (CDW) as it flows down the slope. In recent decades, a freshening has been observed in this outflowing AABW directly downstream at Cape Adare (Gordon et al., 2015; Swift & Orsi, 2012). Along the Adélie Land/George V Land coast,

Table 1
IAPSO SSW Salinity Batch Number and Offsets (Kawano, Aoyama, et al., 2006; Updated Uchida et al., 2018) Used Along Each Occupation of the Eight Sections Considered Here

Line	Year	IAPSO batch	Offset (10^{-3})	Ad hoc offset (10^{-3})
P06	1992	P116	1.4	−0.5
	2003	P142	0.2	0
	2010	P149	0.7	0
	2017	P160	0.0	0
P14	1996	114	2.0	−3.7
	2013	154	0.6	0
P15	1996	P114	2.0	−2.5
	2001	P140	−0.3	0
	2009	P148/P150	0.0/0.7	0
	2016	P156	0.4	0
P16	1992	P108/110/114	1.7/1.9/2.0	−0.5
	2005	P144/145	−0.5/−1.0	0
	2014	P156	0.4	0
P17E	1992	P120	−0.9	0
	2017	159	−0.3	0
P18	1994	114	2.0	0
	2008	147	−0.6	0
	2016	159	−0.3	0
P21	1994	123	0.7	−1.0
	2009	150	0.7	0
S4P[a]	1992	P108	1.7	0.12
	2011	P152	−1.3	0

Note. Additional ad hoc offsets applied to the occupation are also listed (see section 2.1). IAPSO = International Association for the Physical Sciences of the Oceans; SSW = standard seawater.
[a]S4P was occupied in 2018, but the data had not been finalized at the time of this analysis.

freshening has also been observed (Jacobs & Giulivi, 2010; Rintoul, 2007; van Wijk & Rintoul, 2014) with an accelerated freshening and decrease in production reported after the collapse of the Mertz Glacier Tongue (Kobayashi, 2018; Shadwick et al., 2013, 2017; Snow et al., 2018; Tamura et al., 2012, 2016). Regardless of the cause, freshening of AABW accounts for an 84-Gton/year flux of freshwater, reducing the density of the new bottom water (Purkey & Johnson, 2013). In addition, a decrease in oxygen levels of AABW near the Ross Sea has been observed, providing evidence of a decline in abyssal ventilation rates (Ozaki et al., 2009). These changes have been connected to strong water mass freshening and a reduction of the ventilation rate of AABW in the Indo-Pacific sectors of the Southern Ocean (Aoki et al., 2005; Gordon et al., 2015; Johnson et al., 2008; Menezes et al., 2017; Purkey & Johnson, 2013; Shimada et al., 2012; Swift & Orsi, 2012; van Wijk & Rintoul, 2014).

In the deep Pacific basins to the north of the Southern Ocean, consistent warming has been observed starting in the 1990s and continuing into the 2000s (Desbruyères et al., 2016; Fukasawa et al., 2004; Johnson et al., 2007; Kawano, Fukasawa, et al., 2006; Kouketsu et al., 2009; Kouketsu et al., 2011; Purkey & Johnson, 2010; Sloyan et al., 2013), with dynamically driven abyssal warming associated with isotherm displacement observed even in the North Pacific along 47°N between 1985 and 1999 (Fukasawa et al., 2004). The deep and abyssal Pacific Ocean is ventilated primarily by Lower CDW and AABW flowing north in a deep western boundary current along the west side of the Southwest Pacific Basin (Whitworth et al., 1999) through the Samoan Passage and into the Central Pacific Basin (Reid, 1997; Roemmich et al., 1996; Voet et al., 2016). Water flowing northward through the Southwest Pacific Basin generally exceeds a neutral density of 28.2 kg/m^3 and is composed of over 50% AABW (Johnson, 2008; Talley, 2003; Wijffels et al., 2001). Rates of abyssal warming in the Southwest Pacific Basin and North Pacific between the 1990s and 2000s were 1 m°C/year (1 m°C = 1×10^{-3} °C/year) and 0.3 m°C/year, respectively (Desbruyères et al., 2016; Kouketsu et al., 2011; Purkey & Johnson, 2010; Sloyan et al., 2013; Voet et al., 2016).

These previous regional and global estimates of deep and abyssal warming and freshening were mostly limited to decadal repeat ship-based surveys collected between the 1990s and 2000s. Here we add another decade of repeat hydrography to explore the temporal and spatial variability of this warming and freshening in the Pacific Ocean, starting near source regions in the Ross Sea and following AABW as it spreads eastward into the rest of the Amundsen-Bellingshausen Basin and northward into the Southwest Pacific Basin. We discuss the eight repeat hydrographic sections used and analysis methods in section 2. We present results showing a monotonic abyssal warming and increased (in both magnitude and spatial extent) freshening with time in section 3. We discuss the implications of this deep and abyssal Pacific warming and freshening in section 4.

2. Data and Methods

2.1. Data

We analyze full depth conductivity-temperature-depth (CTD) station data collected along eight repeated hydrographic sections spanning the southern Pacific Ocean (Figure 1 and Table 1). All eight sections were first occupied between 1991 and 1996 as part of the World Ocean Circulation Experiment (WOCE) Hydrographic Program and later reoccupied one to three subsequent times between 2001 and 2017 (Table 1), first under the auspices of Climate and Ocean Variability, Predictability, and Change (CLIVAR)/CO_2 and more recently the Global Ocean Ship-based Hydrographic Investigation Program (GO-SHIP). Vertical sections of physical and chemical properties for each of the WOCE occupations are provided in Talley (2007). The sections provide broad spatial coverage, with at least one meridional and one

zonal section across each deep basin considered here (Figure 1). Along each section, CTD profiles are taken from the sea surface to within ~10 m of the bottom every 55 km or closer in regions of steep topography. Only stations falling within 10 km of the original WOCE section tracklines are used, and all sections are referenced by their WOCE (and ongoing GO-SHIP) designator hereafter (Figure 1 and Table 1).

Data considered here were collected to the high WOCE and continuing GO-SHIP standards, with salinity, temperature, and pressure accuracies within ±0.002 or since WOCE ±0.001 °C, ±0.002 PSS-78, and ± 2 dbar, respectively (Hood et al., 2010). Any data without a "good" flag are discarded. All data used here are publicly available from the CLIVAR and Carbon Hydrographic Data Office (https://cchdo.ucsd.edu/). The CTD salinity data were calibrated to the bottle salinities, which were analyzed and calibrated to International Association for the Physical Sciences of the Oceans standard seawater onboard. For more accurate intercruise comparisons of salinity, we applied International Association for the Physical Sciences of the Oceans batch-to-batch salinity offsets (Table 1) following Kawano, Aoyama, et al. (2006) and updated by Uchida et al. (2018).

An additional ad hoc salinity offset is applied to most of the WOCE occupations (Table 1). For each section, the offset was determined by identifying a reference potential temperature surface between 2,000 and 4,000 m with low CFCs, following Purkey and Johnson (2013). The salinity difference between the first and all subsequent occupations along the reference isotherm was calculated, and the mean offset was applied to the first occupation (Table 1). The salinity difference between cruises occupied after 2000 was less than 0.0001; therefore, no salinity offset between GO-SHIP cruises is applied. The salinity ad hoc offset between the WOCE and GO-SHIP cruises ranged from 0.0001 to −0.0037. In all but S4P, the offset was negative, acting to lessen any deep freshening trend; hence, all salinity changes discussed hereafter would be greater by ~0–0.004 if the offsets where not applied (Table 1). The consistency of most WOCE occupations being fresher along the reference potential temperature, chosen to be within the Pacific Deep Water, might be an indication of a freshening trend within this water mass, but that seems unlikely considering that it is very old and well mixed. Furthermore, the magnitude of the offset is not geographically consistent, so without additional evidence of freshening within the Pacific Deep Water, we take the conservative approach of assuming this is a calibration bias instead of a real signal.

2.2. Methods

Using all occupations, we assess deep and abyssal ocean variability by calculating local to basin-scale trends in three quantities: (1) the rate of change in potential temperature (θ) on pressure (P) surfaces ($d\theta/dt(P)$), (2) isotherm displacement or the vertical displacement of isotherm height (h) above the sea floor with time ($dh/dt(\theta)$), and (3) the trend in salinity (S) on isotherms ($dS/dt(\theta)$) indicating a water mass change. Here we use $dS/dt(\theta)$ to evaluate where the changes move off the existing θ-S curve, indicating an advected change. This analysis follows the Bindoff and McDougall (1994) framework but assumes there is no "pure cooling" in the deep ocean. We associate the isotherm displacement term, $d\theta/dt(P)$, with dynamical heave reflecting changes in volume of AABW, where the water mass is given by temperature, rather than advective property changes. We make these assumptions in order to do the analysis using potential temperature, rather than density, for two reasons. First, shelf water salinity has varied, but the temperature trends have been small, related to the expected increase in the temperature of the freezing point of seawater associated with the freshening trend (Jacobs & Giulivi, 2010). Second, isopycnal determination is quite sensitive to errors in salinity. In the abyssal southwest Pacific, the effect on density determination of the instrumental 0.001 °C error in temperature is 28 times less than the 0.002 error in salinity. Thus, by quantifying isotherm displacement instead of isopycnal displacement to diagnose decadal heave changes, we can better separate these two processes.

Here we focus primarily on three regions: (1) the Southwest Pacific Basin lying west of the East Pacific Rise in the southeast Pacific, (2) the Ross Sea defined as the western side of the Bellingshausen Basin with an eastern boundary at 132 °W, corresponding to the eastern edge of a strong zonal temperature gradient at all depths on section S4P which signifies southward flow in the Ross Gyre (Figure 2a), and (3) the Amundsen-Bellingshausen Basin defined as the region east of 132 °W encompassing the Amundsen and Bellingshausen ayssal plains (Figure 1). The basin boundaries are otherwise defined using the shallowest points along a ridge (Smith & Sandwell, 1997), and ridges were chosen such that the abyssal properties in each basin are similar, indicating the basin is ventilated by similar bottom water (Purkey & Johnson, 2010).

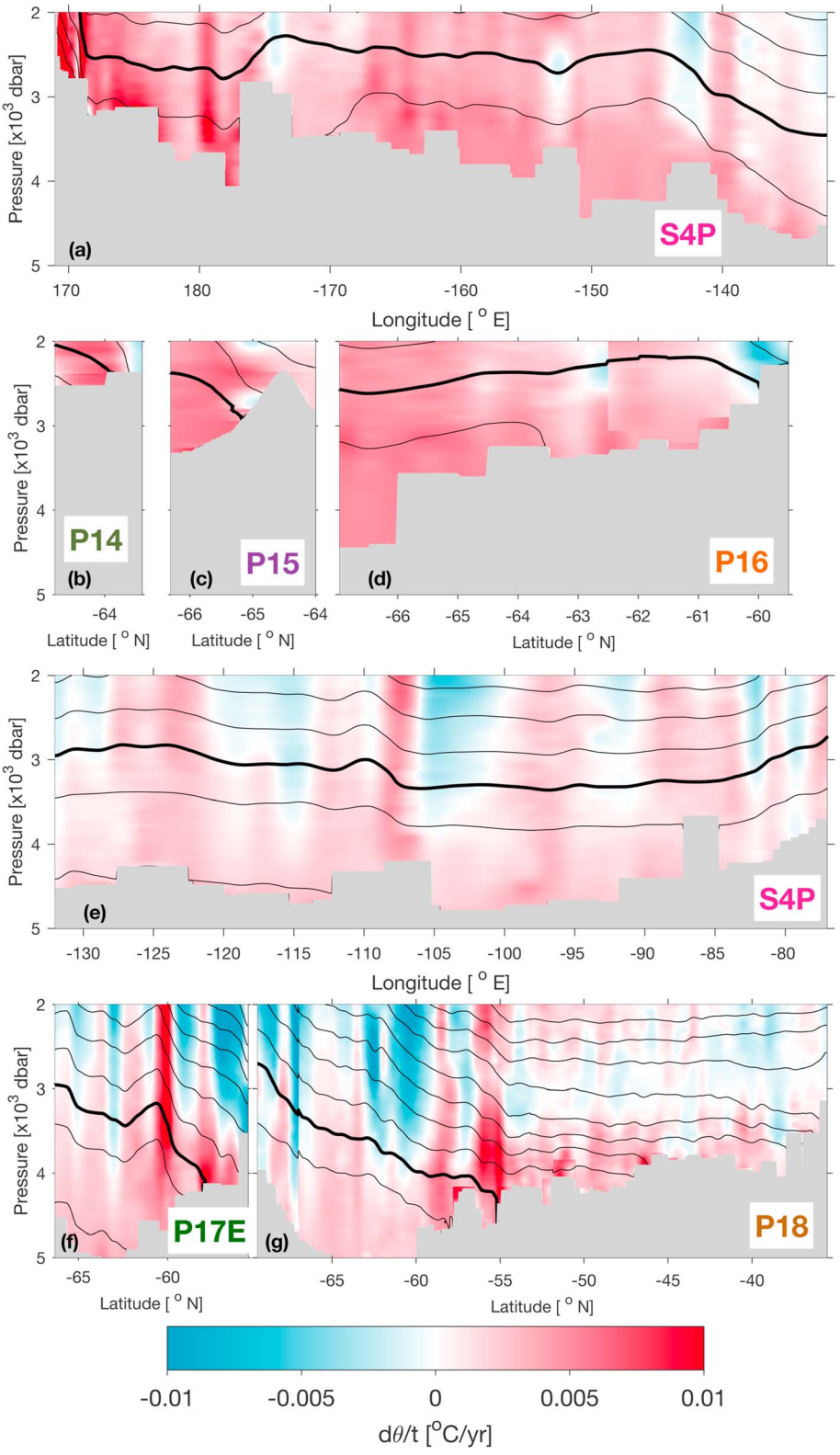

Figure 2. Time rate of change of potential temperature, dθ/dt (color contour; °C/year) along repeated sections within (a–d) the Ross Sea region and (e–g) the Amundsen-Bellingshausen (AB) Basin with mean isotherms contoured at 0.2 °C intervals (black) with the 0.2 and 0.4 °C isotherms highlighted (by thicker contours) in the Ross Sea and Amundsen-Bellingshausen Basin, respectively. See Figure 1 for section locations.

The data are gridded and interpolated following Purkey and Johnson (2010). First, potential temperature and salinity profiles are low-passed vertically with a Hanning filter and interpolated onto a uniform 20-dbar vertical grid. Data along each occupation of each section are interpolated onto a uniform 2-min horizontal latitude or longitude grid. The θ-P (pressure) and S-P data are then interpolated onto a uniform 0.01 °C θ grid. The height above the sea floor of each isotherm is calculated as the difference between $P(\theta)$ and the bottom (Smith & Sandwell, 1997) following Purkey and Johnson (2012).

The along-section and regional means and uncertainties in $d\theta/dt(P)$, $dS/dt(\theta)$, and $dh/dt(\theta)$ are calculated. First, the time rate of change of temperature, isotherm height, and salinity at every vertical and horizontal grid point along each section are calculated as a linear fit between the first occupation and all subsequent occupations following methods in Purkey and Johnson (2010, 2012, 2013; Figures 2 and 3). From those, the mean and variance of $d\theta/dt(P)$, $dS/dt(\theta)$, and $dh/dt(\theta)$ along each section within geographical regions are computed (as shown for $dh/dt(\theta)$ in Figure 4). The basin means and standard deviations for each $d\theta/dt(P)$ and $dS/dt(\theta)$ are then calculated using a length-weighted mean of each section within a basin (Figures 5 and 6). All standard deviations are converted to 95% confidence intervals using Student's t distribution and assuming a horizontal decorrelation length scale of 163 km (Purkey & Johnson, 2010, 2013).

The local contribution of the deep and abyssal warming in each basin to the heat budget and steric SLR is calculated using each basin's mean $d\theta/dt(P)$. First, $d\theta/dt(P)$ is interpolated onto a 20-m vertical depth (z) grid. The local heat flux (Q) and steric SLR (F) across z_i = 2,000, 3,000, 4,000, and 5,000 m are calculated following Purkey and Johnson (2010) as

$$Q = \frac{\int_{\text{bottom}}^{z_i} \rho \cdot C_p \cdot d\theta/dt(z) \cdot a \cdot dz}{a(z_i)}, \text{and} \tag{1}$$

$$F = \frac{\int_{\text{bottom}}^{z_i} \alpha \cdot d\theta/dt(z) \cdot a \cdot dz}{a(z_i)}, \tag{2}$$

where the profiles of density (ρ), specific heat (C_p), and thermal expansion coefficient (α) are calculated from the climatological T and S data for each basin (Gouretski & Koltermann, 2004). The surface area (a) at z_i is calculated using a satellite bathymetric data set (Smith & Sandwell, 1997).

In addition to the multidecadal trend over the entire observational period, we examine the temporal variability in $d\theta/dt(P)$. The differences along each section within a basin are calculated between all sequential occupations when more than two occupations are available (Figure 7). For example, if the section has been occupied three times, the difference in temperature, expressed as a rate by dividing by time between occupations, is calculated using occupation one and two as well as two and three, and three and four (Figure 7) in order to identify variability in the warming rate and test the robustness of a linear trend model.

3. Results

Consistent patterns of ocean warming and freshening are observed within the deep portions of the Ross Sea, Amundsen-Bellingshausen Basin, and Southwest Pacific Basin (Figures 2 and 3). The strongest abyssal warming of 3.5 m°C/year (0.035 °C/year) is observed in the Ross Sea below 4,000 m with smaller, but statistically significant, warmings of 2.5 m°C/year to the east in the Amundsen-Bellingshausen Basin and 1.3 m°C/year to the north in the Southwest Pacific Basin (Figures 2a–2d and 5). Warming in all basins is associated with the sinking (increasing depth) of the coldest isotherms at rates of tens of meters per year throughout the region (Figure 4). These rates become statistically indistinguishable from 0 around the 0.8 °C isotherm in all basins. Water mass freshening is indicated by changes in the slope of the θ-S curves for the various sections. Freshening is observed for waters colder than 0.5 °C in the Ross Sea between the 1990s and the 2010s (Figures 6a and 8a–8c). The freshening is also found to the east in the Amundsen-Bellingshausen Basin between the 1990s and the 2000s, and further between the 1990s and the 2010s (Figures 6b and 8d–8f). In the Southwest Pacific Basin, a bottom-intensified freshening is observed only between the 2000s and the 2010s, for waters colder than 0.68 °C (Figures 6c and 9).

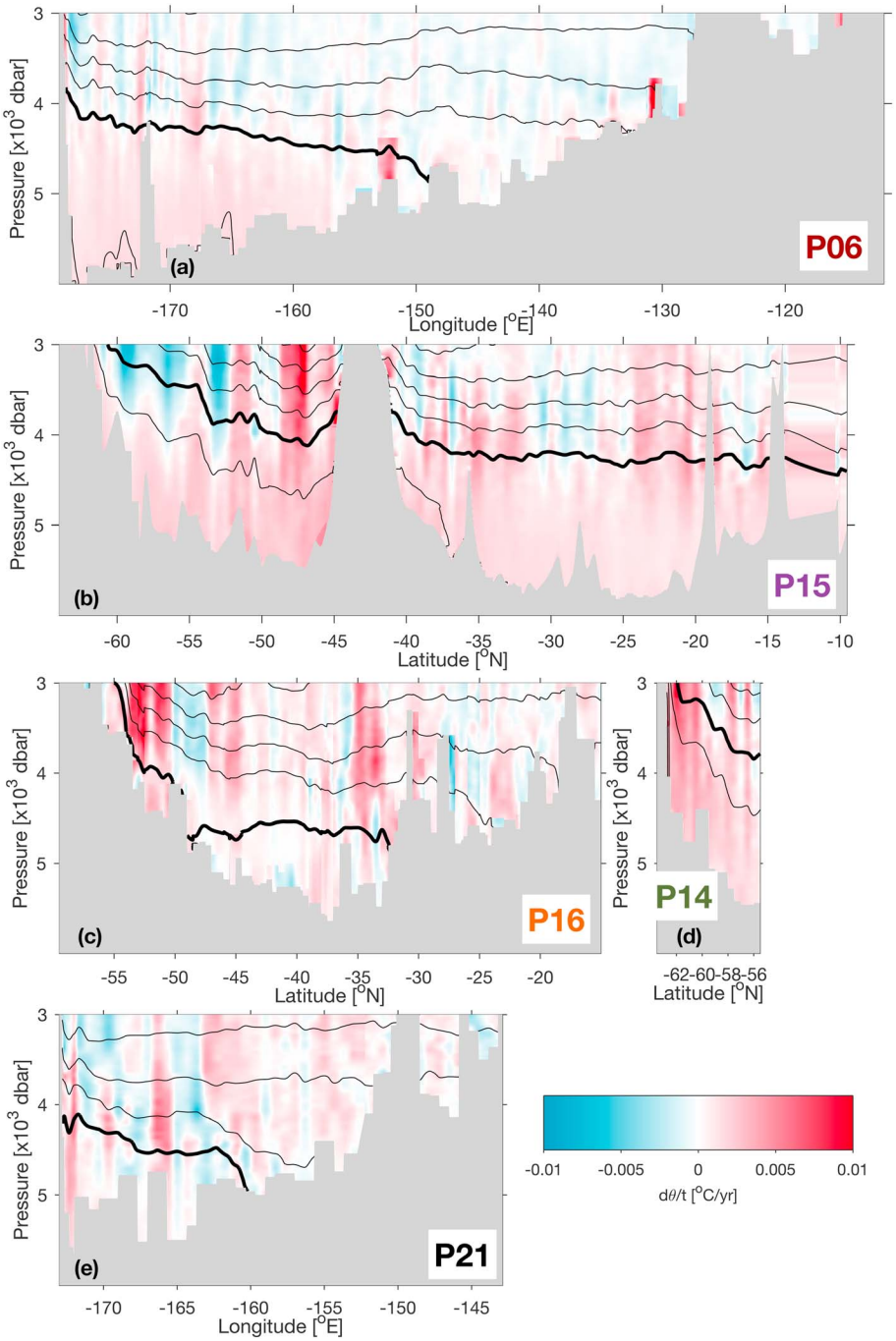

Figure 3. Following Figure 2 for sections within the Southwest Pacific (SWP) Basin with the mean isotherms contoured at 0.2 °C intervals (black) and the 0.8 °C isotherm highlighted (by thicker contours) for reference (a–e). See Figure 1 for location of sections.

3.1. Ross Sea

The abyssal Ross Sea is primarily ventilated by Ross Sea Bottom Water (RSBW; a variety of AABW) formed along the continental slope of the Ross Shelf, located in the southwest corner of the basin (Figure 1). Dense shelf water flows off the shelf within the Drygalski and Challenger troughs, entraining ambient CDW (Jacobs, 2004) to form AABW. The AABW plume follows the coastal current (Gordon et al., 2009; Orsi & Wiederwohl, 2009) with most heading west into the Indian Ocean but some heading north into the Ross Gyre. The Ross Gyre, a strong cyclonic polar gyre which dominates the local circulation, carries AABW

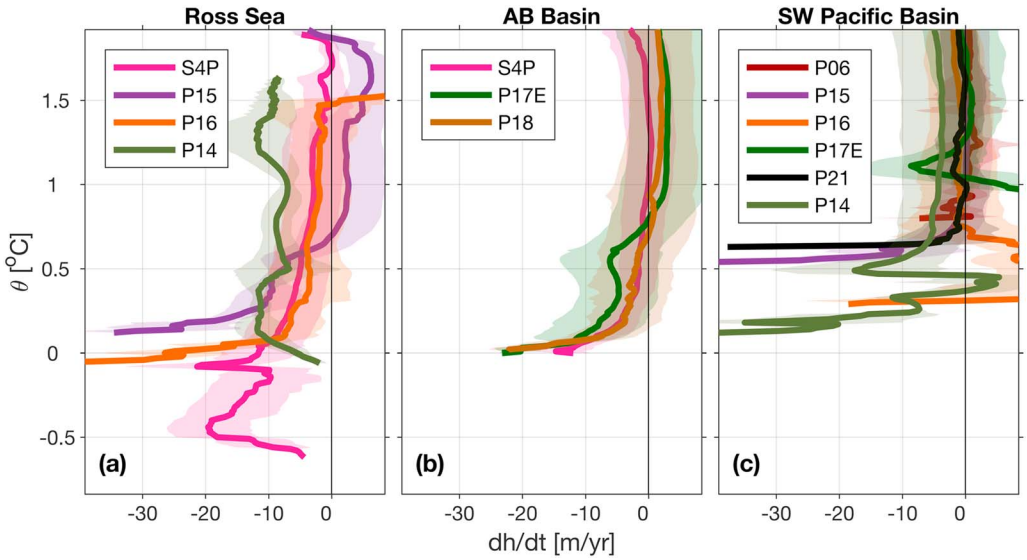

Figure 4. Mean time rate of change of isotherm height with 95% confidence intervals along all sections within the (a) Ross Sea, (b) Amundsen-Bellingshausen (AB) Basin, and (c) Southwest (SW) Pacific Basin. Isotherm height is defined as the distance of a given isotherm above the bottom at each latitude or longitude.

eastward along the southern flank of the Pacific-Antarctic Ridge before turning southward around 132°W, dividing the basin dynamically as seen by the strong slope in isopycnals (Figure 2a). The Antarctic Circumpolar Current fronts are located on the northern side of the Pacific-Antarctic Ridge until the Eltanin and Udintsev Fracture Zones where the fronts cross the ridge, turn south, and travel through the Amundsen-Bellingshausen Basin toward Drake Passage (Orsi et al., 1995). Therefore, the youngest bottom water sampled is along the western end of S4P near Cape Adare followed by the southern ends of P14, P15, and P16, respectively.

Strong property changes in AABW have occurred throughout the abyssal Ross Sea, with the largest magnitudes near the outflow of RSBW sampled along S4P near Cape Adare. This freshening is consistent with an advected water mass change stemming from the 0.003 year^{-1} freshening of the Ross Shelf waters since 1950,

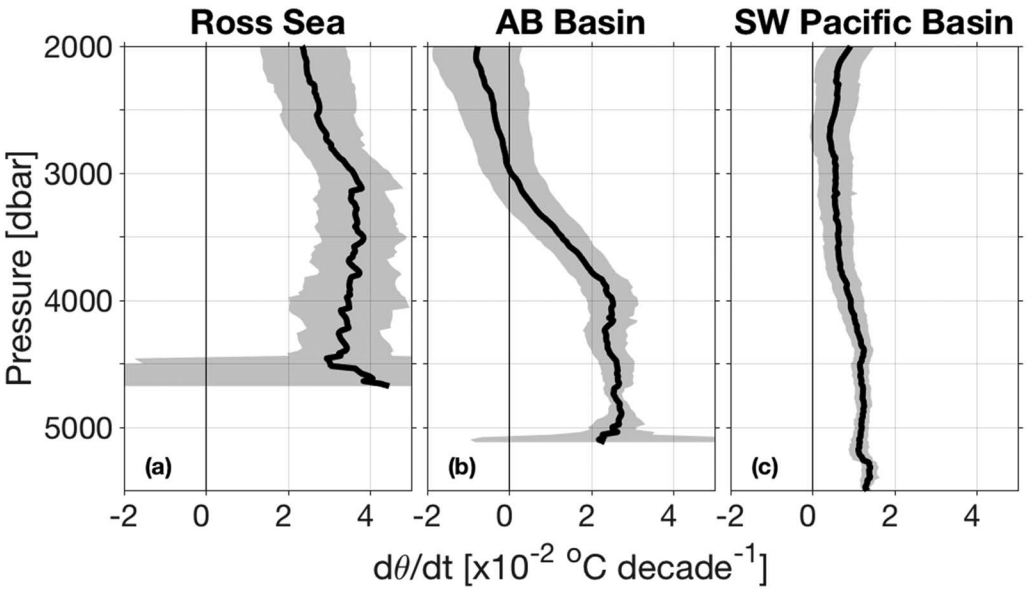

Figure 5. Basin mean time rate of change of potential temperature ($d\theta/dt$) using all occupations of all sections within the (a) Ross Sea, (b) Amundsen-Bellingshausen Basin, and (c) Southwest Pacific Basin, all with 95% confidence intervals (shading).

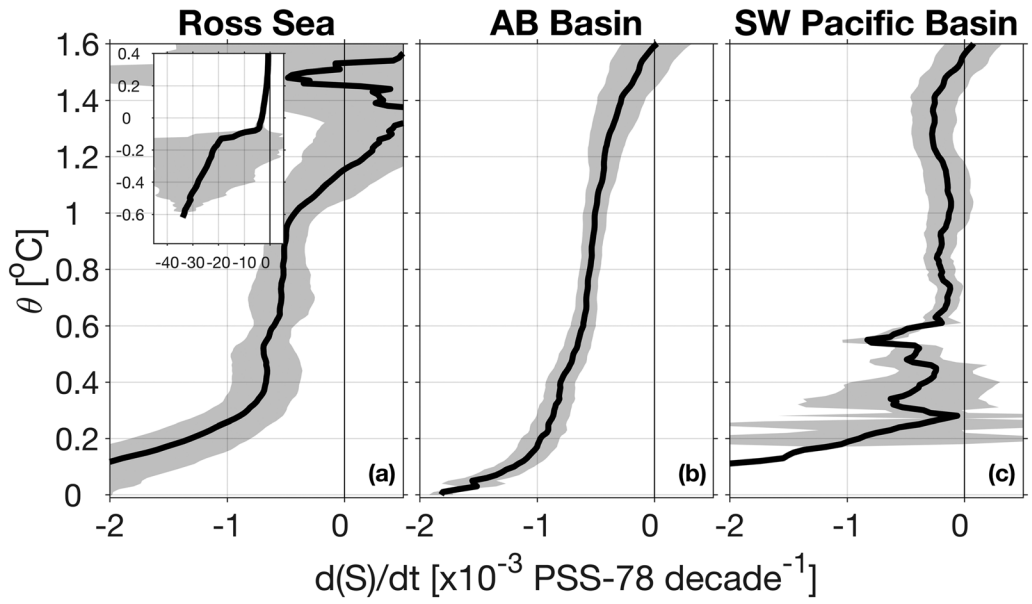

Figure 6. Basin mean rate of change of salinity on potential temperature surfaces with 95% confidence intervals for the (a) Ross Sea, (b) Amundsen-Bellingshausen Basin, and (c) Southwest Pacific Basin. Inset in (a) shows plot of Ross Sea with expanded salinity scale and temperature scale extending from 0.4 °C to below 0.

likely tied to increased glacial melt from West Antarctica (Jacobs, 2002; Jacobs & Giulivi, 2010). The freshening is seen as a strong change in the slope of θ-S relationship from occupation to occupation for $\theta < 0.6$ °C (Figures 8a–8c). An extremely strong freshening of 0.025 ($\pm$0.015) year^{-1} between 1992 and 2011 is observed in the coldest ($\theta < -0.2$ °C) outflow plumes near Cape Adare (Figure 8a), as previously noted in Swift and Orsi (2012). The freshening is strongest in the coldest, youngest water but is detectible across the whole basin

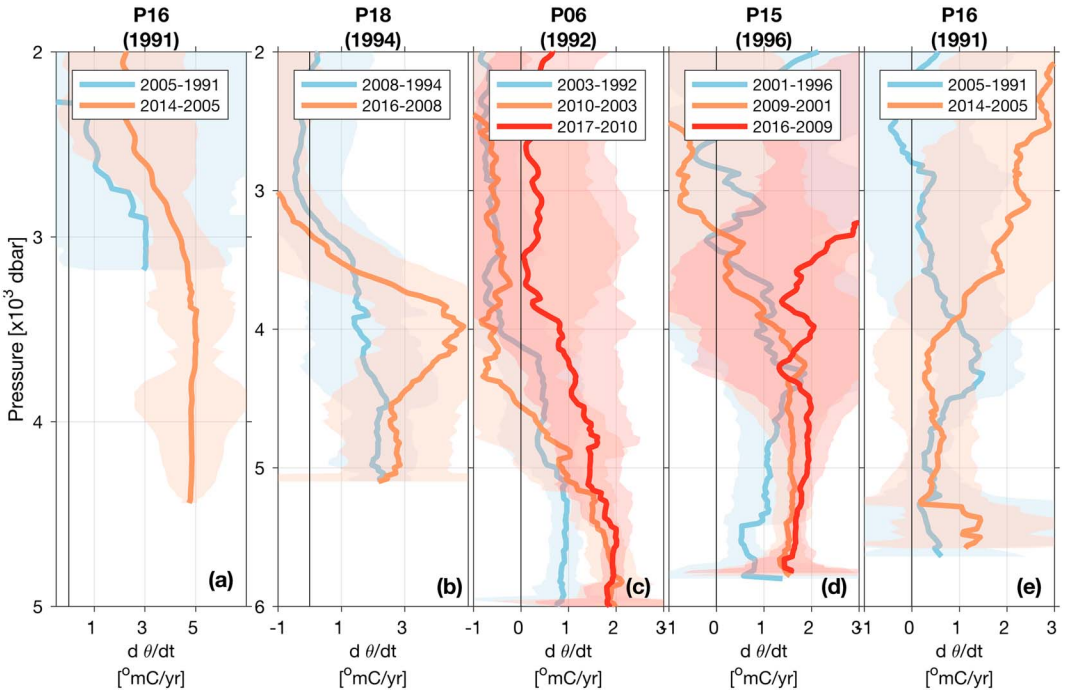

Figure 7. Mean rate of change in potential temperature between all pairs of occupations of (a) P16 across the Ross Sea, (b) P18 across the Amundsen-Bellingshausen Basin, (c) P06 across the Southwest Pacific Basin, (d) P15 across the Southwest Pacific Basin, and (e) P16 across the Southwest Pacific Basin. Potential temperature changes are expressed as a rate by dividing the temperature difference by time between occupations.

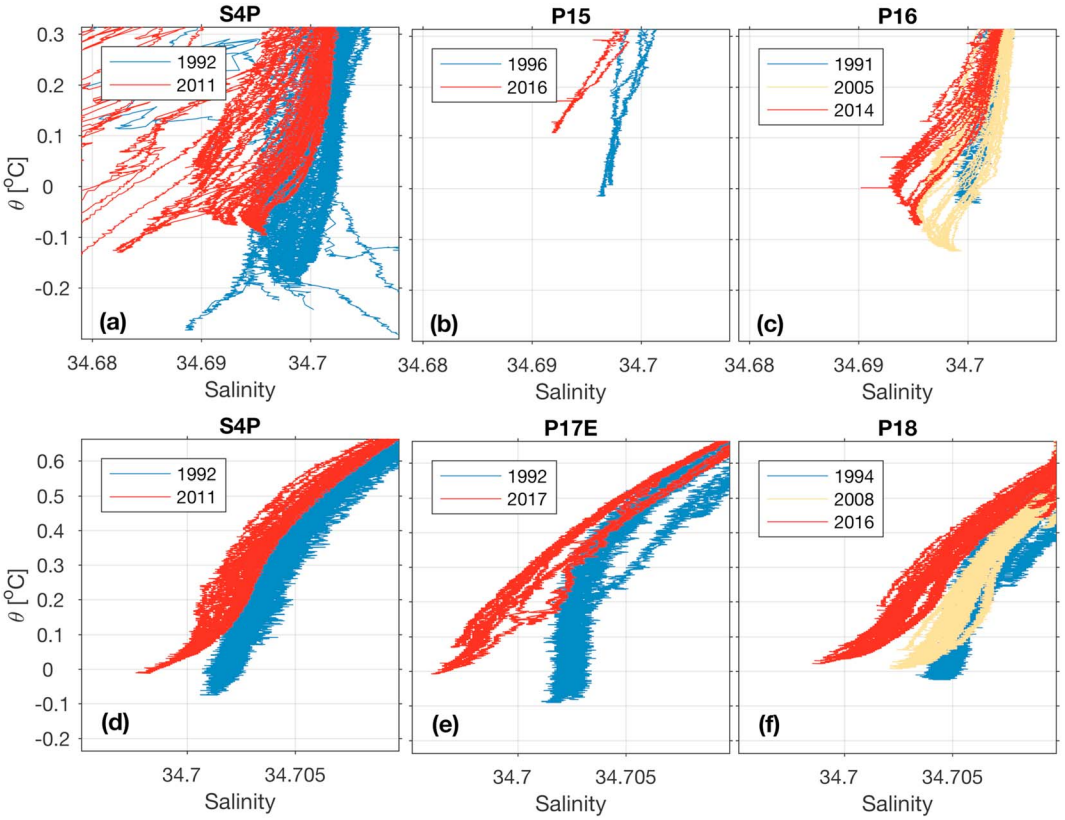

Figure 8. Potential temperature-salinity (θ-S) diagrams from all conductivity-temperature-depth stations along the World Ocean Circulation Experiment (blue) and subsequent Climate and Ocean Variability, Predictability, and Change/CO_2 and Global Ocean Ship-based Hydrographic Investigation Program occupations (yellow and red) of (a) S4P, (b) P15, and (c) P16 within the Ross Sea and (d) S4P, (e) P17E, and (f) P18 within the Amundsen-Bellingshausen Basin (see Figure 1 for location).

(Figures 8a–8c). Following the circulation of AABW around the Ross Gyre, an 0.0015 year^{-1} freshening is seen in P14 between 1996 and 2012 in very cold ($\theta < 0$ °C) waters (Figure 9a), 0.0004 year^{-1} in slightly warmer ($\theta < 0.1$ °C) waters sampled in P15 between 1996 and 2016 (Figure 8b), 0.0003 year^{-1} in P16 data between 2005 and 2014, and 0.0005 year^{-1} in the interior Ross Sea along S4P (Figure 8c). The mean freshening rate of waters colder than 1 °C in the Ross Sea is 0.0009 ($\pm$0.0002) year^{-1} (Figure 6a).

A strong warming driven by isotherm displacement is also observed throughout the Ross Sea below 2,000 m, roughly corresponding to the 0.4 °C isotherm (Figures 2a–2d and 4a). Unlike the freshening, however, the isotherm displacement is more uniform in space with warming at remarkably similar rates observed along all sections from 2,000 m to the bottom (Figures 2a–2d). The warming corresponds to the deepening of isotherms. All four transects: P14, P15, P16, and S4P in the Ross Sea show similar isotherm descents at a rate of 5–15 m/year for $0.1 < \theta < 0.5$ °C, roughly corresponding to a 3,000- to 1,500-m depth range (Figures 2 and 4a). Most sections have a maximum rate >5 m/year for $-0.1 < \theta < 0.1$ °C. All four lines show a slow attenuation of this loss of cold water for $0.5 < \theta < 1$ °C, at which point the change is indistinguishable from 0 outside the 95% confidence interval (Figure 4a). The largest loss of volume at depth with a slow recovery above is indicative of a decrease in cold dense AABW. The temperature class of water replacing this deep loss is in the temperature range of CDW.

Warming is also seen in the newest outflow waters sampled in S4P near Cape Adare but with more variability, likely tied to short-term variations. The coldest waters sampled in the deep basin, $\theta < -0.2$ °C, are confined to the outflow region of AABW and have all descended at rates of ~15 m/year, resulting in a mean warming of 7.8 ($\pm$7.9) m°C/year in that region (95% confidence intervals; Figures 2a and 4a). However, the bottom waters in the coastal current have highly variable outflow with large seasonal cycles (Gordon et al., 2015). In addition, the few stations on P16 that sample "young" cold AABW along the southern

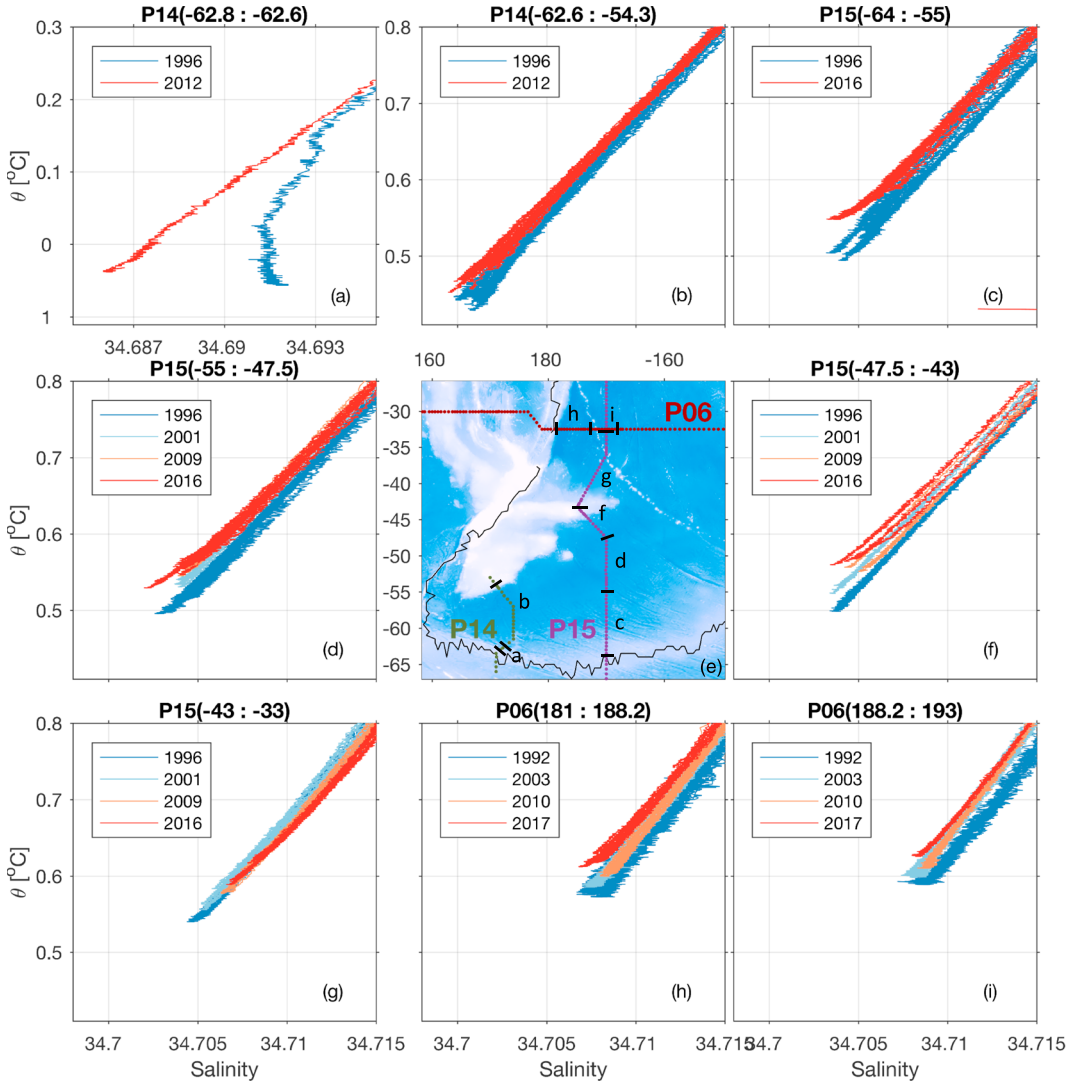

Figure 9. Potential temperature-salinity (θ-S) diagrams from all conductivity-temperature-depth stations along the World Ocean Circulation Experiment (dark blue) and subsequent Climate and Ocean Variability, Predictability, and Change/CO_2 and Global Ocean Ship-based Hydrographic Investigation Program occupations (light blue, orange, and red), for select stations along occupations of (a, b) P14, (c, d, f, g) P15, and (h, i) P06 in the Southwest Pacific Basin. Salinity and potential temperature axes are the same for all panels except (a). Locations of stations used in each panel are shown in (e) with black tick marks indicating division points. Longitude or latitude range is also given in the subplot titles.

flank of the Antarctic-Pacific Rise show large descents in the heights of the coldest isotherms (Figure 4a, orange). The meridional sections on the north end of the basin are within the strong eastward current along the ridge, seen by the strongly tilted isotherms (Figures 2b and 2c), making them susceptible to shorter, surface-forced, variability as the Ross Gyre spins up or down. This variability is not resolved by the decadal surveys analyzed here. Nonetheless, all sections across all occupations show a similar trend, with large isotherm descent of waters for $-0.1 < \theta < 0.1$ °C, relaxing to no descent by $\theta = 1$ °C, providing evidence that the decadal surveys are capturing a long-term trend (Figure 4a) that is not overwhelmed by shorter-term variability.

The Ross Sea has warmed below 2,000 m at a depth mean rate of 2–4 m°C/year (Figure 5a). The area weighted mean warming rate below 2,000 m was 3.3 (±0.9) m°/year between 1992 and 2017 (Table 2). This warming equates to the accumulation of 2.4 (±0.7) MW of heat or an average of 0.7 (±0.2) W/m^2 applied over the 2,000 m isobaths. Furthermore, the warming below 2,000 m causes a 0.7 (±0.2) mm/year local SLR from thermal expansion (Table 2).

Table 2
Heat Flux (W/m^2) Across the Interface Depth Required to Account for the Warming Below (Top), Thermosteric SLR (mm/year) Resulting From Warming Below (Middle), and Mean Warming Rate (m°C/year) Below a Given Interface Depth (Bottom) in the Ross Sea (Ross), Amundsen-Bellingshausen (AB) Basin, and Southwest Pacific (SWP) Basin With Uncertainties at the 95% Confidence Level

	Heat (W/m^2)		
Interface depth (m)	Ross	AB	SWP
2,000	0.66 ± 0.20	0.19 ± 0.20	0.23 ± 0.13
3,000	0.38 ± 0.10	0.25 ± 0.10	0.17 ± 0.07
4,000	0.10 ± 0.03	0.17 ± 0.03	0.12 ± 0.03
5,000	-	-	0.04 ± 0.01
	SLR (mm/year)		
Interface depth (m)	Ross	AB	SWP
2,000	0.70 ± 0.20	0.26 ± 0.22	0.29 ± 0.15
3,000	0.44 ± 0.12	0.33 ± 0.12	0.23 ± 0.08
4,000	0.13 ± 0.04	0.23 ± 0.04	0.17 ± 0.03
5,000	-	-	0.06 ± 0.01
	$d\theta/dt$ (m°C/year)		
Interface depth (m)	Ross	AB	SWP
2,000	3.28 ± 0.92	1.19 ± 0.66	0.94 ± 0.34
3,000	3.55 ± 0.99	1.97 ± 0.54	1.06 ± 0.26
4,000	3.46 ± 1.42	2.53 ± 0.42	1.26 ± 0.19
5,000	-	-	1.34 ± 0.16

Note. SLR = sea level rise.

3.2. Amundsen-Bellingshausen Basin

AABW from the Ross Sea flows eastward along the Pacific-Antarctic Ridge, filling the deep abyssal plains of the Amundsen-Bellingshausen Basin (Figure 1). Below 3,500 m AABW is bathymetrically trapped, unable to continue north or east, and upwells to lighter densities before exiting the basin (Orsi et al., 1999). Deep CTD stations from the early 1990s and before show the high-salinity signature of Ross Sea Bottom Water that occupied most of the deep basin (Orsi et al., 1999).

The Amundsen-Bellingshausen Basin shows a uniform warming and bottom-intensified freshening signal in the relatively homogenous bottom water for $\theta < 0.2$ °C, roughly corresponding to $P > 3{,}500$ dbar (Figures 2e–2g). Below 4,000 m, across all three sections, the AABW has warmed by 3 m°C/year. The warming is equivalent to a 14–21 m/year descent of the 0 °C isotherm and a slower descent extending to $\theta = 0.6$ °C (Figure 4b). The isotherm displacement rate is identical in the meridional (P18) and zonal (S4P) transects across the basin and is consistent between the 1994 and 2008 and between the 2008 and 2016 occupations of P18 (Figures 4b and 7b).

In addition to warming, AABW in the Amundsen-Bellingshausen Basin freshened between the 1990s and 2010s, with a change in the θ-S shape, similar to the Ross Sea (Figures 6b and 8d–8f). For $\theta < 0.3$ °C, the WOCE occupations of S4P, P17E, and P18 had a minimal deep salinity gradient, resulting in mostly a thermally stratified deep layer. A bottom-intensified freshening of 0.0018 decade^{-1} has shifted the θ-S curves fresh in all repeat sections (Figures 8d–8f). Between the WOCE occupations and first repeats of S4P from 1992 to 2011 and P18 from 1994 to 2008, the 0 °C waters freshened by 0.0014 and 0.0015 decade^{-1}, respectively. Between 1992 and 2017 for P17E and between 2008 and 2016 for P18, the freshening rate accelerated to 0.0024 and 0.0025 decade^{-1}, respectively. The warming and freshening both act to decrease the deep density stratification for $\theta < 0.2$ °C. The basin mean deep freshening below 0.2 °C was 0.0013 (±0.0001) decade^{-1} (Figure 6b). However, for $\theta > 0.2$ °C there is a small, 0.0006 (±0.0001) decade^{-1} freshening trend extending through multiple water masses on both S4P and P18, indicating a possible salinity offset between cruises (Figure 6b). If this is a bias, correcting it would decrease the freshening trends discussed above by 0.0006 decade^{-1}.

Overall, the Amundsen-Bellingshausen Basin has warmed at a mean rate of 2.5 (±0.4) m°C/year for $P > 4{,}000$ dbar between 1992 and 2017 (Table 2, Figure 5b). While the warming rate is constant for $P > 4{,}000$ dbar, there is a steady decrease with decreasing depth such that warming is statistically indistinguishable from 0 by 3,200 dbar (Figure 5b). This pattern indicates strong warming in regions filled with AABW with little change in those occupied by CDW. The net warming for $P > 4{,}000$ dbar is equivalent to a heat flux of 0.17 (±0.03) W/m^2 across the 4,000-m isobath and a local thermal steric SLR of 0.23 (±0.04) mm/year (Table 2). The local heat flux is about 3 times the expected heat flux from abyssal geothermal heating (Davies & Davies, 2010; Hamza et al., 2008). We know of no evidence indicating that local geothermal heating has increased over the past three decades, making geothermal energy an unlikely source of the observed changes.

3.3. Southwest Pacific Basin

Bottom water in the Southwest Pacific Basin primarily enters from the Australian-Antarctic Basin through deep sills south of New Zealand. AABW flows north in a strong deep western boundary current (Whitworth et al., 1999) and circulates throughout the deep basin (Reid, 1997). The inflowing water is mostly warmer than 0.4 °C with a small amount of colder water entering from the Ross Sea and Amundsen-Bellingshausen Basin through deep fracture zones along the Pacific-Antarctic Ridge (Reid, 1997), as seen in the southernmost stations of P14 (Figures 3d and 9a). The sill constraint causes the abyssal properties to be relatively homogenous in the basin, with isotherms that gently slope down to the east and north.

While the bottom waters found here are warmer than traditional AABW, having mixed with overlying deep waters as they spread north, they are still composed of over 70% AABW with direct ties to both RSBW and Adélie Land Bottom Water (Johnson, 2008).

Waters of $\theta < 0.8$ °C (~$P > 4{,}000$ dbar) have warmed throughout the basin, driven by isotherm displacement (Figures 3, 4c, and 5c). In most sections, uniform warming occurs for $\theta < 0.8$ °C (Figure 3). At P14, the inflowing water shows a statistically significant warming of 1.6 (±0.32) m°C/year for $P > 4{,}000$ dbar (Figure 3d). The abyssal warming is seen throughout the deep western boundary current (P15, Figure 3b) and across the zonal section at 32°S (P06, Figure 3a) below 0.8 °C. The warming is less consistent in the bottom waters found in the eastern and northern ends of the basin (Figure 3).

The basin mean warming rate is 1.26 (±0.19) m°C/year for $P > 4{,}000$ m using all occupations and all sections (Table 2). The large amount of data and the low variability in space and time across the basin contribute to the small 95% confidence limits. This warming is equivalent to a local heat flux of 0.12 (±0.03) W/m^2 and a thermosteric SLR of 0.17 (±0.03) mm/year. The warming found shallower than 4,000 m slowly decreases with decreasing depth but stays statistically significant up to 2,700 m (Figure 5c). Including the warming between 4,000 and 2,000 m would increase the net heat flux to 0.23 (±0.13) W/m^2 and the local SLR to 0.29 (±0.15) mm/year (Table 2).

The abyssal warming is associated with isotherm displacement. The height of the abyssal isotherms between 0.5 and 0.7 °C across P14 have fallen at a rate of 8–18 m/year suggesting that the temperature of the bottom water flowing into the basin is warmer (Figure 4c). In all sections, the coldest waters of 0.5–0.65 °C found during WOCE have disappeared. The abyssal basin is now composed of water with temperatures between 0.6 and 0.8 °C (Figure 4c).

Unlike the Ross Sea and Amundsen-Bellingshausen Basin to the south, there was no observable basin-wide change in the θ-S relationship in the Southwest Pacific Basin from the 1990s to the 2010s, indicating no basin-wide water mass freshening in AABW here during that time interval (Figure 9). However, there is a subtle change in the slope of the θ-S curves in the 2010s relative to the 2000s in the most recently ventilated water in the deep western boundary current, indicative of small freshening for $\theta < 0.65$ °C (Figures 6c, 9c, and 9d). While the freshening in the Ross Sea and Amundsen-Bellingshausen Basin is indicated only for waters of $\theta < 0.5$ °C (Figures 8), those fresher bottom waters mix with warmer deep waters above as they work their way through passes and over sills into the Southwest Pacific Basin, diluting but also mixing that freshening signal up to slightly warmer potential isotherms on the way north.

Where could this small freshening be coming from? The AABW freshening from the Ross and Adélie Land formation regions has been previously reported through the Australian-Antarctic Basin that feeds the Southwest Pacific Basin (e.g., Johnson et al., 2008; Menezes et al., 2017; Purkey & Johnson, 2013; Shimada et al., 2012; van Wijk & Rintoul, 2014) and, therefore, this signal could be a delayed freshening slowly advecting northward through the traditional pathway of AABW to the Pacific. Alternatively, a more direct flow of AABW through deep fracture zones in the Pacific-Antarctic Ridge could be contributing (Figure 1). The repeated single station along P14°S at 62.7°S, on the north ridge of a deep fracture zone in the Pacific-Antarctic Ridge, sampled waters colder than 0 °C in both occupations, indicating northward flow from the Ross Sea into the Southwest Pacific Basin there (Figure 9a). Furthermore, this water freshened by 0.005 between 1996 and 2012, suggesting that this pathway is directly bringing fresher AABW into the basin from the Ross (Figure 9a). Regardless of the pathway, the freshening detected along the southern end of the most recent occupation of P15 provides evidence that abyssal freshening has reached the Southwest Pacific Basin.

3.4. Recent Acceleration in the Deep Warming Rate

We test the temporal consistency of the warming rate by calculating the mean section-warming rate between individual occupations using the five sections with three or more occupations (Figure 7).

In the southern basins, only two sections, P16 in the Ross Sea and P18 in the Amundsen-Bellingshausen Basin, have had a third occupation (Figures 7a and 7b). (GO-SHIP occupied S4P again in 2018, but that data set was not available at the time of this analysis.) The warming rates agree within their 95% confidence intervals among all occupation pairs in waters deeper than 2,000 m. In addition, the vertical structure of the warming pattern is identical, indicating that the pattern of decreasing volume of AABW compensated by

an increasing volume of CDW is consistent in time. The mean warming rates calculated for P16 2005–2014 (Figure 7a, orange) and P18 2008–2017 (Figure 7b, orange) are both slightly higher than those calculated for P16 1992–2005 (Figure 7a, blue) and P18 1994–2008 (Figure 7b, blue) but overlap within 95% confidence intervals.

The rate of AABW warming may have accelerated in the Southwest Pacific Basin, with stronger warming between the 2000s and the 2010s than between the 1990s and the 2000s (Figures 7c–7e). Rates of deep and abyssal warming calculated along individual sections with more than two occupations were always higher between the 2000s and 2010s than between the 1990s and the 2000s. The mean warming rate along P15, which follows the DWBC, was 1 m°C/year between 1992 and 2003, accelerating to a statistically significant faster rate of 1.7 m°C/year between 2001 and 2009 and staying high at 1.7 m°C/year between 2009 and 2016 (Figure 7d). Similarly, the warming rate along P06 at 32°S below 5,000 m was 1 m°C/year between 1992 and 2003 but doubled to 2 m°C/year between 2003 and 2010 and between 2010 and 2017 (Figure 7c). This accelerated warming is consistent with the faster warming rate of 3 (+/−1) mC/year between mid-2014 and late 2018 measured by the Deep Argo floats in the Southwest Pacific Basin (Johnson et al., 2019). While not statistically significant, the warming rates along P16 in the eastern side of the basin also were larger between 2014 and 2005 than between 2005 and 1991 at most but not all depths (Figure 7e). In addition, the warming rate in the deep ocean between 2,000 and 4,000 m is highest between the most recent occupations of P06, P15, and P16.

4. Summary and Discussion

Warming of Antarctic Bottom Waters has been previously found between the 1990s and the 2000s by analysis of repeat hydrographic sections taken in those two decades (e.g., Purkey & Johnson, 2010). Here analyzing repeat hydrographic sections from a third decade, we report continued bottom water warming into the 2010s in the South Pacific Ocean (Figure 1), with rates highest in the Ross Sea, 3.46 (±1.42) m°C/year, followed by the Amundsen-Bellingshausen Basin to the east, 2.53 (±0.42) m°C/year, and then the Southwest Pacific Basin to the north, 1.26 (±0.19) m°C/year, (Figure 5 and Table 2). Warming rates from the 2000s to the 2010s in the Southwest Pacific Basin have accelerated relative to the rates from the 1990s to the 2000s (Figure 7). This acceleration is in contrast to the Southwest Atlantic, where near-bottom warming in the Argentine Basin, strong from 1989 to 2005, was reduced or absent from 2005 to 2014, although warming continued in the abyssal Brazil Basin (Johnson et al., 2014). Bottom water warming is associated with a freshening for $\theta < 0.5$ °C in the Ross Sea and the Amundsen-Bellingshausen Basin from the 1990s through the 2000s and into the 2010s (Figures 6 and 8). However, in the Southwest Pacific Basin, freshening of waters for $\theta < 0.65$ °C is discernible only between the 2000s and the 2010s (Figure 9c). The warming is associated with a reduction in the volumes of the coldest bottom waters in all basins, with isotherms descending at rates of tens of meters per year (Figure 4).

The warming and freshening of the bottom waters in the South Pacific are likely associated with a freshening of the Ross shelf waters since 1950 (Jacobs & Giulivi, 2010), which are an important component of the AABW there. This freshening substantially increases the buoyancy of these waters, perhaps reducing the formation rate of AABW in addition to making it less dense. Such changes are communicated fastest into adjacent and then remote deep ocean basins by planetary waves, which effect changes in depths of isopycnals, but no water mass changes (e.g., Masuda et al., 2010). The slower communication of these changes is by advection, which can include water mass changes, and increases in concentrations of transient tracers such as CFCs and SF_6 (Purkey et al., 2018). The Ross Sea, closest to the AABW formation region, shows the largest water mass changes, a steady freshening in waters of $\theta < 0.5$ °C from the 1990s onward (Figures 8a–8c). The Amundsen-Bellingshausen Basin, still relatively close to the formation region, also shows freshening for waters of $\theta < 0.5$ °C, although of smaller amplitude (Figures 8d and 8e). However, the Southwest Pacific Basin, more distant, and separated from the bottom water formation region by mid-ocean ridges, shows freshening for waters of $\theta < 0.65$ °C from the 2000s to the 2010s but not from the 1990s to the 2000s (Figures 9c, 9d, and 9f).

One might argue that this apparent freshening "delay" is explained by the difference in distance along the main paths of AABW, but CFCs were detected in AABW during the WOCE P15 revisit in 1996 (McTaggart & Johnson, 1997), meaning at least some part of the near-bottom water mass reaching the

Southwest Pacific Basin in 1996 had been ventilated after the 1970s. Comparison of salinity on P06 and P15S in this basin on the isopycnal (neutral) surfaces also showed freshening between the 2000s and 1990s (Figures 21 and 29 of Katsumata & Fukasawa, 2011; Sloyan et al., 2013). These observations can be explained if AABW in the Southwest Pacific Basin is transported across a topographic barrier, or "sill," consistent with the much warmer (> 0.5 °C, Figures 9d–9i) and saltier (>34.7) bottom water found in this basin than in the Ross Sea. Salinity increases upward toward the Lower CDW maximum (of North-Atlantic Deep Water origin) around 4,000 dbar. Because the AABW isotherms are deepening (Figure 4), the water mass that negotiates the sill becomes warmer and saltier. Given a typical rate of 10-m descent per year (Figure 4), the increases in a decade in potential temperature and salinity are approximately 0.04 °C and 0.002, respectively, where the background stratifications are 0.4 m°C/m for temperature (Figure 3) and 2×10^{-5} m^{-1} for salinity (WOCE Atlas P15S sections; Talley (2007)). This salinity increase can well be compensated by the water mass freshening (Figure 6), leaving an upward shift of the θ-S diagram (Figure 9). Alternatively, the route or source of AABW to the Southwest Pacific Basin could have changed, delivering a fresher variety of AABW from the Indian or Atlantic sector in the most recent decade.

Here we have shown that the AABW throughout the South Pacific has warmed, with a possible slight acceleration in the most recent decade. The warming is accompanied by a clear bottom-intensified freshening, strongest in the Ross Sea and Amundsen-Bellingshausen Basin, but with early signs of the arrival of a fresher variety of AABW to the Southwest Pacific Basin seen in the 2016/2017 occupations of P15 and P06. The warming for $P > 4{,}000$ m is equivalent to an accumulation of energy at a rate of 3.5 ($\pm$0.1) MW in the deep ocean and drives a local SLR of 0.14 ($\pm$0.04) mm/year from thermal expansion, making it an important contributor to ocean heat uptake and SLR. These changes reflect a shift in the deep ocean ventilation and circulation, but the driving mechanisms are still poorly understood.

In order to resolve this important climate signal, continuous global monitoring of the full water column through a combination of GO-SHIP's repeat hydrography and Deep Argo is needed. While Argo floats now routinely sample the upper half of the ocean volume year-round, and first reached sparse global coverage around 2005 (Lyman & Johnson, 2014), the global ocean below 2,000 m depth is currently primarily sampled through global decadal repeat surveys made under the auspices of GO-SHIP (Talley et al., 2016). The results we present suggest that bottom water warming in the South Pacific is relatively steady from the 1990s through the 2010s; however, there is a hint of acceleration in the warming and northward progression of the freshening water mass change. Furthermore, other deep basins have exhibited more substantial time variability (e.g., Johnson et al., 2014), and future decades are expected to bring more warming to the deep ocean (Bryan et al., 2014; Rhein et al., 2013). A proposed global array of about 1,200 Deep Argo floats would greatly improve our ability to estimate deep and abyssal ocean changes such as those reported here, as well as variations in circulation, in closer to real time (Johnson et al., 2015, 2019). Some progress is being made toward that vision, with regional pilot arrays of Deep Argo floats established in the south Indian, South Pacific, and North Atlantic oceans (Jayne et al., 2017), with plans for the South Atlantic Ocean as well.

Acknowledgments

S. G. P. was supported by a U.S. GO-SHIP postdoctoral fellowship through NSF grant OCE-1437015, which also supported L. D. T. and S. M. and collection of U.S. GO-SHIP data since 2014 on P06, S4P, P16, and P18. G. C. J. is supported by the Global Ocean Monitoring and Observation Program, National Oceanic and Atmospheric Administration (NOAA), U.S. Department of Commerce and NOAA Research. B. M. S and S. E. W. were supported by the Australian Government Department of the Environment and CSIRO through the Australian Climate Change Science Programme and by the National Environmental Science Program. We are grateful for the hard work of the science parties, officers, and crew of all the research cruises on which these CTD data were collected. We also thank the two anonymous reviewers for their helpful comments that improve the manuscript. This is PMEL contribution 4870. All CTD data sets used in this analysis are publicly available at the website (https://cchdo.ucsd.edu).

References

Aoki, S., Rintoul, S. R., Ushio, S., Watanabe, S., & Bindoff, N. L. (2005). Freshening of the Adélie land bottom water near 140 E. *Geophysical Research Letters*, *32*, L23601. https://doi.org/10.1029/2005GL024246

Bindoff, N. L., & McDougall, T. J. (1994). Diagnosing climate change and ocean ventilation using hydrographic data. *Journal of Physical Oceanography*, *24*(6), 1137–1152. https://doi.org/10.1175/1520-0485(1994)024<1137:DCCAOV>2.0.CO;2

Bryan, F. O., Gent, P. R., & Tomas, R. (2014). Can Southern Ocean eddy effects be parameterized in climate models? *Journal of Climate*, *27*(1), 411–425. https://doi.org/10.1175/JCLI-D-12-00759.1

Davies, J. H., & Davies, D. R. (2010). Earth's surface heat flux. *Solid Earth*, *1*(1), 5–24. https://doi.org/10.5194/se-1-5-2010

Desbruyères, D. G., Purkey, S. G., McDonagh, E. L., Johnson, G. C., & King, B. A. (2016). Deep and abyssal ocean warming from 35 years of repeat hydrography. *Geophysical Research Letters*, *43*, 10,356–10,365. https://doi.org/10.1002/2016GL070413

Durack, P. J., Gleckler, P. J., Purkey, S. G., Johnson, G. C., Lyman, J. M., & Boyer, T. P. (2018). Ocean warming: From the surface to the deep in observations and models. *Oceanography*, *31*(2), 41–51. https://doi.org/10.5670/oceanog.2018.227

Fukasawa, M., Freeland, H., Perkin, R., & Watanabe, T. (2004). Bottom water warming in the North Pacific Ocean. *Nature*, *427*(6977), 825–827. https://doi.org/10.1038/nature02337

Gordon, A. L., Huber, B., & Busecke, J. (2015). Bottom water export from the western Ross Sea, 2007 through 2010. *Geophysical Research Letters*, *42*, 5387–5394. https://doi.org/10.1002/(ISSN)1944-8007

Gordon, A. L., Orsi, A. H., Muench, R., Huber, B. A., Zambianchi, E., & Visbeck, M. (2009). Western Ross Sea continental slope gravity currents. *Deep Sea Research Part II: Topical Studies in Oceanography*, *56*(13–14), 796–817. https://doi.org/10.1016/j.dsr2.2008.10.037

Gouretski, V. V., & Koltermann, K. P. (2004). WOCE global hydrographic climatology. Berichte des Bundesamtes für Seeschifffahrt und Hydrographie, 35, pp. 52 + 2 CD-ROMs.

Hamza, V., Cardoso, R., & Neto, P. C. (2008). Spherical harmonic analysis of the Earth's conductive heat flow. *International Journal of Earth Sciences*, *97*, 205–226.

Hood, E. M., Sabine, C. L., & Sloyan, B. M., (Eds.) (2010). The GO-SHIP repeat hydrography manual: A collection of expert reports and guidelines. IOCCP Report Number 14, ICPO Publication Series Number 134. Retrieved from https://www.go-ship.org/HydroMan.html

Jacobs, S. S. (2002). Freshening of the Ross Sea during the late 20th century. *Science*, *297*(5580), 386–389. https://doi.org/10.1126/science.1069574

Jacobs, S. S. (2004). Bottom water production and its links with the thermohaline circulation. *Antarctic Science*, *16*(4), 427–437. https://doi.org/10.1017/S095410200400224X

Jacobs, S. S., & Giulivi, C. F. (2010). Large multidecadal salinity trends near the Pacific–Antarctic continental margin. *Journal of Climate*, *23*(17), 4508–4524. https://doi.org/10.1175/2010JCLI3284.1

Jayne, S. R., Roemmich, D., Zilberman, N., Riser, S. C., Johnson, K. S., Johnson, G. C., & Piotrowicz, S. R. (2017). The Argo program: Present and future. *Oceanography*, *30*(2), 18–28. https://doi.org/10.5670/oceanog.2017.213

Johnson, G. C. (2008). Quantifying Antarctic Bottom Water and North Atlantic deep water volumes. *Journal of Geophysical Research*, *113*, C05027. https://doi.org/10.1029/2007JC004477

Johnson, G. C., Lyman, J. M., & Loeb, N. G. (2016). Improving estimates of Earth's energy imbalance. *Nature Climate Change*, *6*, 639–640. https://doi.org/10.1038/nclimate3043

Johnson, G. C., Lyman, J. M., & Purkey, S. G. (2015). Informing deep Argo array design using Argo and full-depth hydrographic section data. *Journal of Atmospheric and Oceanic Technology*, *32*, 2178–2198. https://doi.org/10.1175/JTECH-D-15-0139.1

Johnson, G. C., McTaggart, K. E., & Wanninkhof, R. (2014). Antarctic Bottom Water temperature changes in the western South Atlantic from 1989 to 2014. *Journal of Geophysical Research: Oceans*, *119*, 8567–8577. https://doi.org/10.1002/2014JC010367

Johnson, G. C., Mecking, S., Sloyan, B. M., & Wijffels, S. E. (2007). Recent bottom water warming in the Pacific Ocean. *Journal of Climate*, *20*, 5365–5375. https://doi.org/10.1175/2007JCLI1879.1

Johnson, G. C., Purkey, S. G., & Bullister, J. L. (2008). Warming and freshening in the abyssal southeastern Indian Ocean. *Journal of Climate*, *21*, 5351–5363. https://doi.org/10.1175/2008JCLI2384.1

Johnson, G. C., Purkey, S. G., Zilberman, N. Z., & Roemmich, D. (2019). Deep Argo quantifies bottom water warming rates in the Southewest Pacific Basin. *Geophysical Research Letters*, *46*. https://doi.org/10.1029/2018GL081685

Katsumata, K., & Fukasawa, M. (2011). Changes in meridional fluxes and water properties in the Southern Hemisphere subtropical oceans between 1992/1995 and 2003/2004. *Progress in Oceanography*, *89*(1–4), 61–91. https://doi.org/10.1016/j.pocean.2010.12.008

Kawano, T., Aoyama, M., Joyce, T., Uchida, H., Takatsuki, Y., & Fukasawa, M. (2006). The latest batch-to-batch difference table of standard seawater and its application to the WOCE one time sections. *Journal of Oceanography*, *62*, 777–792.

Kawano, T., Fukasawa, M., Kouketsu, S., Uchida, H., Doi, T., Kaneko, I., et al. (2006). Bottom water warming along the pathway of lower circumpolar deep water in the Pacific Ocean. *Geophysical Research Letters*, *33*, L23613. https://doi.org/10.1029/2006GL027933

Kawase, M. (1987). Establishment of deep ocean circulation driven by deep-water production. *Journal of Physical Oceanography*, *17*, 2294–2307. https://doi.org/10.1175/1520-0485(1987)017<2294:EODOCD>2.0.CO;2

Khatiwala, S., Primeau, F., & Holzer, M. (2012). Ventilation of the deep ocean constrained with tracer observations and implications for radiocarbon estimates of ideal mean age. *Earth and Planetary Science Letters*, *325*, 116–125. https://doi.org/10.1016/j.epsl.2012.01.038

Kobayashi, T. (2018). Rapid volume reduction in Antarctic Bottom Water off the Adélie/George V land coast observed by deep floats. *Deep Sea Research Part I: Oceanographic Research Papers*, *140*, 95–117. https://doi.org/10.1016/j.dsr.2018.07.014

Kouketsu, S., Doi, T., Kawano, T., Masuda, S., Sugiura, N., Sasaki, Y., Toyoda, T., et al. (2011). Deep ocean heat content changes estimated from observation and reanalysis product and their influence on sea level change. *Journal of Geophysical Research*, *116*, C03012. https://doi.org/10.1029/2010JC006464

Kouketsu, S., Fukasawa, M., Kaneko, I., Kawano, T., Uchida, H., Doi, T., et al. (2009). Changes in water properties and transports along 24°N in the North Pacific between 1985 and 2005. *Journal of Geophysical Research*, *114*, C01008. https://doi.org/10.1029/2008JC004778

Lyman, J. M., & Johnson, G. C. (2014). Estimating global ocean heat content changes in the upper 1800 m since 1950 and the influence of climatology choice. *Journal of Climate*, *27*, 1946–1958. https://doi.org/10.1175/JCLI-D-12-00752.1

Masuda, S., Awaji, T., Sugiura, N., Matthews, J. P., Toyoda, T., Kawai, Y., et al. (2010). Simulated rapid warming of abyssal North Pacific waters. *Science*, *329*(5989), 319–322. https://doi.org/10.1126/science.1188703

McTaggart, K., & Johnson, G. (1997). CTD/O_2 measurements collected on a climate and global change cruise (WOCE sections P14S and P15S) during January–March, 1996. NOAA Data Report ERL PMEL-63 (pp. 485).

Menezes, V. V., Macdonald, A. M., & Schatzman, C. (2017). Accelerated freshening of Antarctic Bottom Water over the last decade in the southern Indian Ocean. *Science Advances*, *3*(1), e1601426. https://doi.org/10.1126/sciadv.1601426

Orsi, A. H., Johnson, G. C., & Bullister, J. L. (1999). Circulation, mixing, and production of Antarctic Bottom Water. *Progress in Oceanography*, *43*(1), 55–109. https://doi.org/10.1016/S0079-6611(99)00004-X

Orsi, A. H., Whitworth, T. III, & Nowlin, W. D. Jr. (1995). On the meridional extent and fronts of the Antarctic Circumpolar Current. *Deep Sea Research Part I: Oceanographic Research Papers*, *42*(5), 641–673.

Orsi, A. H., & Wiederwohl, C. L. (2009). A recount of Ross Sea waters. *Deep-Sea Research Part II: Topical Studies in Oceanography*, *56*, 778–795.

Ozaki, H., Obata, H., Naganobu, M., & Gamo, T. (2009). Long-term bottom water warming in the north Ross Sea. *Journal of Oceanography*, *65*(2), 235–244. https://doi.org/10.1007/s10872-009-0022-z

Palmer, M. D., Roberts, C. D., Balmaseda, M., Chang, Y. S., Chepurin, G., Ferry, N., et al. (2017). Ocean heat content variability and change in an ensemble of ocean reanalyses. *Climate Dynamics*, *49*(3), 909–930. https://doi.org/10.1007/s00382-015-2801-0

Purkey, S. G., & Johnson, G. C. (2010). Warming of global abyssal and deep Southern Ocean waters between the 1990s and 2000s: Contributions to global heat and sea level rise budgets. *Journal of Climate*, *23*, 6336–6351. https://doi.org/10.1175/2010JCLI3682.1

Purkey, S. G., & Johnson, G. C. (2012). Global contraction of Antarctic Bottom Water between the 1980s and 2000s. *Journal of Climate*, *25*, 5830–5844. https://doi.org/10.1175/JCLI-D-11-00612.1

Purkey, S. G., & Johnson, G. C. (2013). Antarctic Bottom Water warming and freshening: Contributions to sea level rise, ocean freshwater budgets, and global heat gain. *Journal of Climate*, *26*, 6105–6122. https://doi.org/10.1175/JCLI-D-12-00834.1

Purkey, S. G., Smethie, W. M., Gebbie, G., Gordon, A. L., Sonnerup, R. E., Warner, M. J., & Bullister, J. L. (2018). A synoptic view of the ventilation and circulation of Antarctic Bottom Water from chlorofluorocarbons and natural tracers. *Annual Review of Marine Science*. https://doi.org/10.1146/annurev-marine-121916-063414

Reid, J. L. (1997). On the total geostrophic circulation of the Pacific Ocean: Flow patterns, tracers, and transports. *Progress in Oceanography*, *39*, 263–352. https://doi.org/10.1016/0079-6611(86)90036-4

Rhein, M., Rintoul, S. R., Aoki, S., Campos, E., Chambers, D., Feely, R. A., et al. (2013). Observations: Ocean. In T. F. Stocker, et al. (Eds.), *Climate change 2013: The physical science basis. Contribution of Working Group I to the Fifth Assessment Report of the Intergovernmental Panel on Climate Change* (pp. 255–316). Cambridge, UK and New York: Cambridge University Press.

Rintoul, S. R. (2007). Rapid freshening of Antarctic Bottom Water formed in the Indian and Pacific oceans. *Geophysical Research Letters*, *34*, L06606. https://doi.org/10.1029/2006GL028550

Roemmich, D., Hautala, S., & Rudnick, D. (1996). Northward abyssal transport through the Samoan passage and adjacent regions. *Journal of Geophysical Research*, *101*(C6), 14,039–14,055. https://doi.org/10.1029/96JC00797

Shadwick, E. H., Rintoul, S. R., Tilbrook, B., Williams, G. D., Young, N., Fraser, A. D., et al. (2013). Glacier tongue calving reduced dense water formation and enhanced carbon uptake. *Geophysical Research Letters*, *40*, 904–909. https://doi.org/10.1002/grl.50178

Shadwick, E. H., Tilbrook, B., & Currie, K. I. (2017). Late-summer biogeochemistry in the Mertz Polynya: East Antarctica. *Journal of Geophysical Research: Oceans*, *122*, 7380–7394. https://doi.org/10.1002/2017JC013015

Shimada, K., Aoki, S., Ohshima, K. I., & Rintoul, S. R. (2012). Influence of Ross Sea Bottom Water changes on the warming and freshening of the Antarctic Bottom Water in the Australian-Antarctic Basin. *Ocean Science*, *8*(4), 419–432. https://doi.org/10.5194/os-8-419-2012

Sloyan, B. M., Wijffels, S. E., Tilbrook, B., Katsumata, K., Murata, A., & Mcdonald, A. (2013). Deep ocean changes near the western boundary of the South Pacific Ocean. *Journal of Physical Oceanography*, *43*, 2132–2141. https://doi.org/10.1175/JPO-D-12-0182.1

Smith, W. H. F., & Sandwell, D. R. (1997). Global seafloor topography from satellite altimetry and ship depth sounding. *Science*, *277*, 1956–1962.

Snow, K., Rintoul, S. R., Sloyan, B. M., & Hogg, A. M. (2018). Change in dense shelf water and Adélie Land Bottom Water precipitated by iceberg calving. *Geophysical Research Letters*, *45*, 2380–2387. https://doi.org/10.1002/2017GL076195

Swift, J., & Orsi, A. H. (2012). Sixty-four days of hydrography and storms: RVIB Nathaniel B. Palmer's 2011 S04P Cruise. *Oceanography*, *25*(3), 54–55. https://doi.org/10.5670/oceanog.2012.74

Talley, L. D. (2003). Shallow, intermediate, and deep overturning components of the global heat budget. *Journal of Physical Oceanography*, *33*(3), 530–560. https://doi.org/10.1175/1520-0485(2003)033<0530:SIADOC>2.0.CO;2

Talley, L. D. (2007). In M. Sparrow, P. Chapman, & J. Gould (Eds.), *Hydrographic atlas of the World Ocean Circulation Experiment (WOCE). Volume 2: Pacific Ocean*. Southampton, UK: International WOCE Project Office. https://doi.org/10.21976/C6WC77

Talley, L. D., Feely, R. A., Sloyan, B. M., Wanninkhof, R., Baringer, M. O., Bullister, J. L., et al. (2016). Changes in ocean heat, carbon content, and ventilation: A review of the first decade of GO-SHIP global repeat hydrography. *Annual Review of Marine Science*, *8*, 185–215. https://doi.org/10.1146/annurev-marine-052915-100829

Talley, L. D., Pickard, G. L., Emery, W. J., & Swift, J. H. (2011). In L. D. Talley, G. L. Pickard, W. J. Emery, & J. H. Swift (Eds.), *Descriptive physical oceanography* (6th ed, 560 pp.). Boston: Elsevier/Academic Press. https://doi.org/10.1016/B978-0-7506-4552-2.10010-1

Tamura, T., Ohshima, K. I., Fraser, A. D., & Williams, G. D. (2016). Sea ice production variability in Antarctic coastal polynyas. *Journal of Geophysical Research: Oceans*, *121*, 2967–2979. https://doi.org/10.1002/2015JC011537

Tamura, T., Williams, G. D., Fraser, A. D., & Ohshima, K. I. (2012). Potential regime shift in decreased sea ice production after the Mertz Glacier calving. *Nature Communications*, *3*, 826.

Uchida, H., Katsumata, K., & Doi, T. (2018). WHP I10 revisit in 2015 data book, JAMSTEC, Yokosuka, Kanagawa, Japan. https://doi.org/10.17596/0000002

Voet, G., Alford, M. H., Girton, J. B., Carter, G. S., Mickett, J. B., & Klymak, J. M. (2016). Warming and weakening of the abyssal flow through Samoan Passage. *Journal of Physical Oceanogrpahy*, *46*, 2389–2401. https://doi.org/10.1175/JPO-D-16-0063.1

Whitworth, T. III, Warren, B. A., Nowlin, W. D. Jr., Rutz, S. B., Pillsbury, R. D., & Moore, M. I. (1999). On the deep western-boundary current in the southwest Pacific Basin. *Progress in Oceanography*, *43*, 1–54.

Wijffels, S. E., Toole, J. M., & Davis, R. (2001). Revisiting the South Pacific subtropical circulation: A synthesis of World Ocean Circulation Experiment observations along 32°S. *Journal of Geophysical Research*, *106*, 19,481–19,513. https://doi.org/10.1029/1999JC000118

van Wijk, E. M., & Rintoul, S. R. (2014). Freshening drives contraction of Antarctic Bottom water in the Australian Antarctic Basin. *Geophysical Research Letters*, *41*, 1657–1664. https://doi.org/10.1002/2013GL058921